Nuclear Instruments and Methods in Physics Research A 787 (2015) 265–269

Contents lists available at ScienceDirect

Nuclear Instruments and Methods in Physics Research A

journal homepage: www.elsevier.com/locate/nima

A new technique of characterization of intrapixel response dedicated to astronomical detectors

C. Ketchazo [a,*], T. Viale [b], O. Boulade [a], G. Druart [b], V. Moreau [a], L. Mugnier [b], D. Dubrueil [a], S. Derelle [b], S. Ronayette [a], N. Guérineau [b], M. Berthé [a]

[a] Service d'Astrophysique, CEA Saclay, Orme des Mérisiers, Gif-sur-Yvette 91191, France
[b] ONERA, The French Aerospace Lab, F-91761 Palaiseau, France

ARTICLE INFO

Available online 23 December 2014

Keywords:
Intra-pixel sensitivity variations
Pixel response function
Talbot effect
CSIG
Modulation transfer function (MTF)

ABSTRACT

This paper is devoted to the presentation of a new technique of characterization of the intra-pixel sensitivity variations (IPSVs) of astronomical detectors. The IPSV is the spatial variation of the pixel response function (PRF). In the case of under-sampled instruments for high quality imaging and accurate photometry, IPSV can contribute to the instrument global error and it should be considered carefully. Our measurement technique is based in the Fourier transform (FT) approach. It consists into the sampling of the pixel transfer function (PTF) by projecting high-resolution periodic patterns onto the whole sensor without classic optics but using the self-imaging property (the Talbot effect) of a continuously self imaging grating (CSIG) illuminated by a plane wave. The PRF is determined by computing the inverse FT. Our measurement technique permits to determine the PRF with a resolution of pixel/10 (10 times Nyquist frequency).

1. Introduction

The impacts of the IPSVs (intra-pixel sensitivity variations) are not negligible in undersampled instruments aimed to carry high quality images and precise photometry. In the InfraRed Array Camera (Spitzer Telescope) for example, the sub-pixel variations is the major source of errors [1]. And largely for applications where a high precision is required, the IPSV must be evaluated and corrected if necessary from the final results. The IPSV measurement can be realized either on final camera systems or by the characterization of the detectors subsystems. On camera systems, the determination of the PRF (pixel response function: the spatial map of the sensitivity across the pixel) involves dithering the camera by a fraction of a pixel over a sequence of exposures. It is then possible to observe how the structure of the objects in the image varies with respect to their positions on the pixel grid. The reconstructed point spread function (PSF) which is the convolution of the optical PSF with the pixel response can be evaluated at any desired fractional pixel location to generate a table of photometric corrections as a function of the relative PSF centroid [1,2] . In laboratory conditions, the characterization of the detectors consists of the projection of an optical probe onto the detector and the measurement of the response of the pixels. Kavaldjiev [3] scanned a front-illuminated charge coupled devices (FI-CCD) with a small light beam (0.4–0.5 μm in diameter). They showed difference in response between pixels. Piterman [4] scanned a back-illuminated CCD using a light beam with 1.7–3.1 μm full width half maximum (FWHM) and the bands B, V, I and a narrow one at 470 μm. They showed that the IPSVs are smoother and less wavelength dependent compared with that for front illuminated CCD them over several pixels. They attributed the difference to the interaction of the light with the gate structures in FI devices. Toyozumi [5] demonstrated that the PRF also depends on the numerical aperture of the incoming beam. In the Near InfraRed (NIR) range, Barron [6] and Biesiadzinski [7] developed a "spots projection" system "the spots-o-matic" to achieve a two-dimensional scan of pixels in a detector by simultaneously projecting the image of 160k small pinholes onto the detector and then scanning them over several pixels.

These different test benches require high quality, precise and stable opto-mechanical devices. The profiles of the projected probes have to be known and controlled precisely in order to be deconvolved from the measurements. And eventually, these measurements are time consuming.

This paper presents an original approach for the measurement of spatial response of the detectors. The measurement technique is presented at Section 2. In Section 3, a description of the measurement procedures is made and in Section 4, the results are presented—we show that with one acquisition, we can evaluate the pixel transfer function and pixel response function until 10 times the Nyquist frequency.

* Corresponding author. Tel.: +33169087573.
E-mail address: christian.ketchazo@cea.fr (C. Ketchazo).

http://dx.doi.org/10.1016/j.nima.2014.12.048
0168-9002/

2. Description of our IPSV measurement technique

The technique we present is based on the Fourier transform (FT) approach and consists in sampling of the pixel transfer function (PTF). The PTF describes the pixel filtering effects (as the modulation transfer function (MTF) does in optics field). To sample the PTF, our approach consists to project high-resolution periodic patterns onto the sensor using the self-imaging property (known as the Talbot effect) of a continuously self-imaging grating (CSIG) illuminated by a plane wave [8] (Fig. 1).

The CSIG is a nondiffracting object developed by ONERA [9,10]. When it is illuminated by a plane wave, a CSIG produces a field whose intensity profile (interferogram) is a propagation and wavelength-invariant biperiodic array of bright spots known as non diffracting arrays (NDA). The figure below illustrates the propagation of the waves diffracted by the CSIG.

In theory to get the NDAs, the grating is defined, in the Fourier domain (FD), by the intersection between the first circle of Montgomery and a Cartesian grid of pitch equal to the inverse of the CSIG period $1/a_0$. The intersection defines N peaks of Dirac also known as the order of the CSIG. Then in the FD, the transmittance of the grating can be mathematically defined as:

$$T_{\mathrm{CSIG}}\left(f_x,f_y\right)=\sum_{k=1}^{N} c_k\delta\left(f_x-\frac{p_k}{a_0},\ f_y-\frac{q_k}{a_0}\right) \tag{1}$$

where c_k are the complex Fourier coefficients. $p_k^2/a_0^2+q_k^2/a_0^2=\eta^2/a_0^2$ and η is a CSIG parameter. The transmission, the PSF and optical transfer function (OTF) of the CSIG are respectively given by:

$$t_{\mathrm{CSIG}}(x,y)=\sum_{k=1}^{N} c_k \exp\left(2i\pi\frac{x\times p_k+y\times q_k}{a_0}\right) \tag{2}$$

$$\mathrm{PSF}_{\mathrm{CSIG}}(x,y)=|t_{\mathrm{CSIG}}(x,y)|^2 \tag{3}$$

and

$$\mathrm{OTF}\left(f_x,f_y\right)=\mathrm{FT}(\mathrm{PSF}_{\mathrm{CSIG}}(x,y)) \tag{4}$$

Considering Eq. (3), one can notice that the PSF is not linked to the wavelength of the light and is not depend on the position z along the propagation. The PSF is achromatic and propagation invariant.

Our objective is to determine the PRF of the detectors at a spatial frequency equal to 10 times the Nyquist frequency, i.e. 1/10 pixel. In the case of the characterization of the e2v CCD-204 for which the pixel is 12 μm, it corresponds to excite a distribution of spatial frequencies with a cutoff value equal at least to 416 mm^{-1} ($10/2p_{\mathrm{ech}}$, p_{ech} is the pixel pitch). Then to design the appropriated CSIG, we suppose a subsampling factor of 12 (1/12 pixel). Then the cutoff frequency of the CSIG must be equal to at least 500 mm^{-1}. We consider the size of the PRF support at $Kp_{\mathrm{ech}}\times Kp_{\mathrm{ech}}$ where K is typically equal to 2 or 3. Finally, the selected CSIG diffracts 48 orders which correspond to 1153 spatial frequencies with the maximum value, ν_c=511 mm^{-1}. The CSIG period is equal to a_0=380 μm with the parameter η equal to $\sqrt{9425}$.

Fig. 2 is the image of the one elementary cell (one period) of the PSF of the CSIG. The bright spot at the center has a radius equal to 1.5 μm.

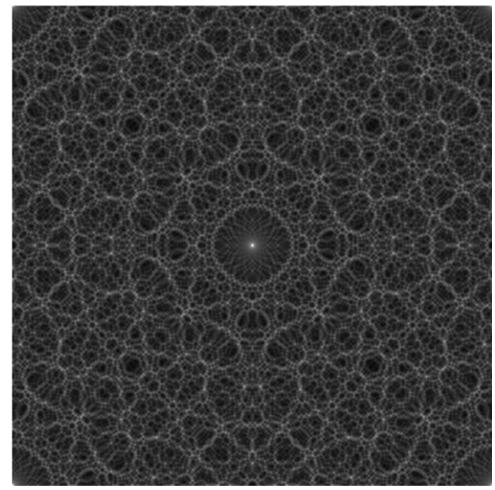

Fig. 2. Point spread function (PSF) of the 48-orders CSIG.

In Fig. 3, the MTF of the CSIG is represented. The MTF is composed by N'discrete spatial frequencies with

$$N'=\frac{N^2}{2}+1=1153 \tag{5}$$

All theses frequencies are located inside a cutoff frequency ring with the maximum value υ_c given by:

$$\upsilon_c=\frac{2\eta}{a_0} \tag{6}$$

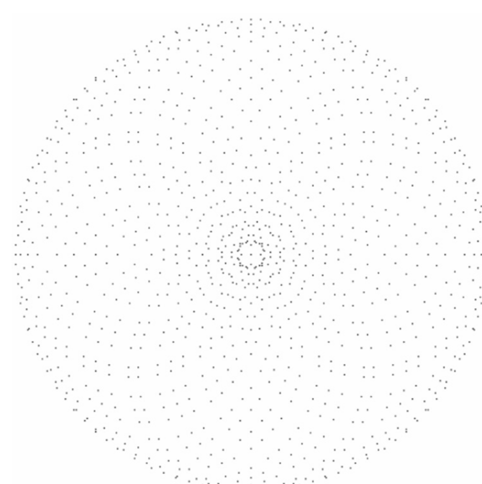

Fig. 3. Modulation transfer function (MTF) of the 48-orders CSIG.

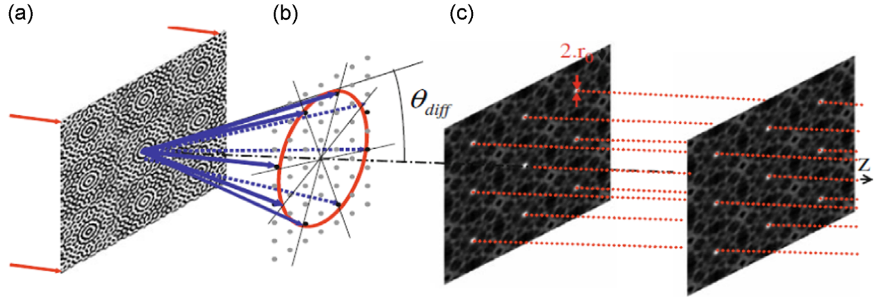

Fig. 1. Illustration of (a) a CSIG, (b) the waves diffracted by the CSIG (blue arrows, whose extremities rely on a circle), and (c) the propagation invariant image produced by the CSIG. (For interpretation of the references to color in this figure legend, the reader is referred to the web version of this article.)

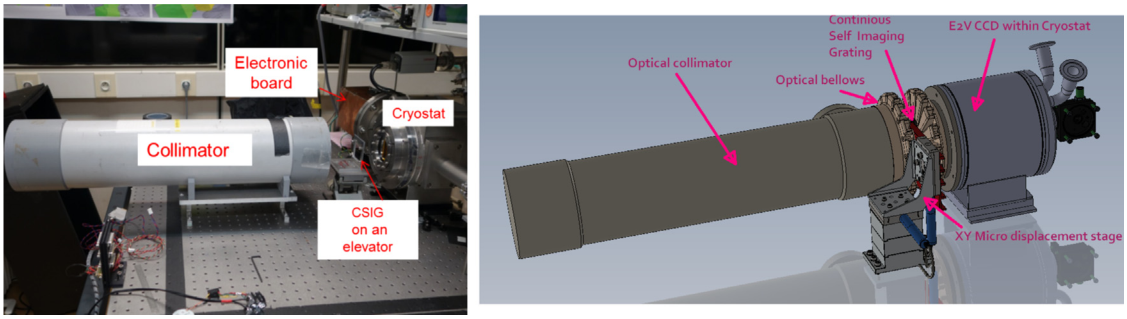

Fig. 4. In left, the experimental setup. In right, a photograph of the test bench. The CSIG is in front of the detector which is mounted inside a cryostat and cooled to reduce the dark current.

The MTF is composed of a central peak of relative weight N, N peaks of relative weight 1 located of the cutoff frequency ring and $N^2/2-N$ other peaks of relative weight 2 located inside the cutoff frequency ring.

The frequencies excite discrete spatial responses on the detector and then permit to sample the PTF of the detector. The PTF is recovered from sparsely sample data by interpolation in the FD. Then we made the assumptions that the spatial spectrum of the pixels is smooth and the repartition of the CSIG peaks is sparsely located on a regular grid.

3. Measurement procedures and preliminary results

The images of the test bench are presented in Fig. 4. The light source is placed at the focus of the collimator (an off-axis paraboloid mirror). The plane waves created illuminate the CSIG which is placed in front off the detector to test. The high-resolution patterns of the grating are projected onto the detector without optics. The optical elements and alignment budgets of our test bench are very low, thanks to the CSIG which no require to be placed at any precise focusing distance between the collimator and the detector. The light source is a Luxeon white LED and it is located at the focus of the collimator. The size of the source is defined by a pinhole.

The CCD is $1\text{k} \times 4\text{k}$ pixel each of 12 μm pitch and is located in the cryostat where it is cooled at 153 K.

The output image from the detector can be expressed as the convolution between the response function of the detector (the pixel response function, PRF) and the PSF of the CSIG. In the FD, the expression of the image can be written as:

$$I\left(f_x, f_y\right) = \text{PTF}\left(f_x, f_y\right) \times \text{PinHoleTF}\left(f_x, f_y\right) \times \text{OTF}\left(f_x, f_y\right) \tag{7}$$

where we suppose, for the purposes of evaluation, a noiseless scenario.

As shown in Eq. (7), the choice of the diameter of the pinhole has to be chosen with a great care to reduce its effects. If the pinhole is too large, it adds an undesired filtering effect in the final image with a cutoff frequency lower than υ_c and in the other hand, if the diameter is too small the SNR will decrease. Finally, we reach to a good tradeoff with pinhole diameter of 0.05 mm. In our test bench, it corresponds to a cutoff frequency equal to 591 mm^{-1} which is larger than the CSIG highest frequency. Therefore, the influence of the pinhole can be neglected and Eq. (7) can be written as:

$$I\left(f_x, f_y\right) = \text{PTF}\left(f_x, f_y\right) \times \text{OTF}\left(f_x, f_y\right) \tag{8}$$

where

$$\text{OTF}\left(f_x, f_y\right) = \sum_{k=1}^{N'} D_k^{\text{in}} \delta\left(f_x - \frac{p'_k}{a_0},\ f_y - \frac{q'_k}{a_0}\right) \tag{9}$$

$$I\left(f_x, f_y\right) = \sum_{k=1}^{N'} D_k^{\text{out}} \delta\left(f_x - \frac{p'_k}{a_0},\ f_y - \frac{q'_k}{a_0}\right) \tag{10}$$

D_k^{in} and D_k^{out} are Fourier coefficients.

And the PTF is deduced by the inverse filter.

$$\text{PTF}\left(f_x, f_y\right) = \frac{D_k^{\text{out}}}{D_k^{\text{in}}} \tag{11}$$

And the mean PRF is obtained by computing the inverse FT of the PTF($f_x f_y$).

4. Preliminary results

The image delivered by the detector is given in Fig. 5.

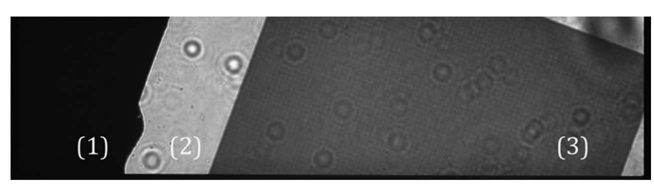

Fig. 5. An output image of the CCD. The zone (1) is the top of the detector and is out of the field covered by the grating. The zone (2) in the bright grey level corresponds to the CSIG holder and the zone (3) is the image of CSIG.

During the acquisition, the CSIG is canted in regard of the CCD lines and columns then the aliased frequencies can fold into frequencies of null amplitude.

In the self-image of the CSIG (zone 3), one can notice the presence of dusts and stripes. These defects would be due to the imperfections of the optical elements and/or interfaces encountered by the light during its propagation. As shown in Fig. 6, these defects introduce non-homogeneities in the image. We also notice that the image is blurred because the interferogram is not well sampled by the CCD.

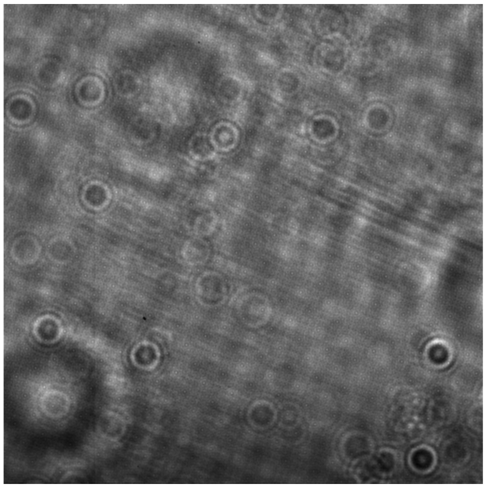

Fig. 6. Image of an area of 512 × 512 pixel.

Nevertheless, the long time illumination images present sufficient contrast to compute the PRF.

To compute properly the PRF, we have to consider all the distribution of the spatial frequencies (Fig. 3), which is equivalent to consider at least a period of the pattern ($380 \times 380\ \mu m^2$). Then, the test bench permits to compute almost naturally the average characteristics of the detectors. Ultimately, we plan to implement a new measurement procedure to determine the characteristic of each individual pixel of a detector. We discuss about this improvement in “Perspectives” section.

In the following paragraphs, the results for an average pixel (corresponding to a zone of 512 × 512 pixels) are given and discussed.

4.1. Pixel transfer function of the average pixel

The PTF is the primary transfer curve used to quantified charge diffusion problems. The PTF describes the ability of the detector to reproduce the contrast modulation present in the scene at any given frequency.

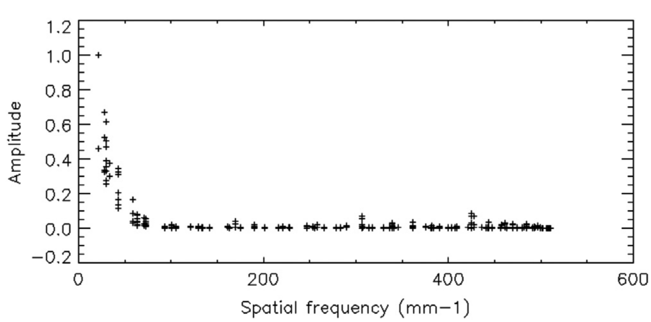

Fig. 7. PTF curve. We neglect the effect of the pinhole.

The curve of the PTF computed at the discrete distribution of spatial frequencies is presented in Fig. 7. The PTF drops rapidly to 0 just before 100 mm^{-1} and takes the value 0.35 at the Nyquist frequency (41 mm^{-1}). We attribute the non-zero values after pixel sampling frequency mostly to the aliased frequencies.

4.2. The pixel response function of the average pixel

The PRF is determined by computing the inverse FT. At Fig. 8, it is represented in contours levels. The physical size of the pixel is materialized by the square.

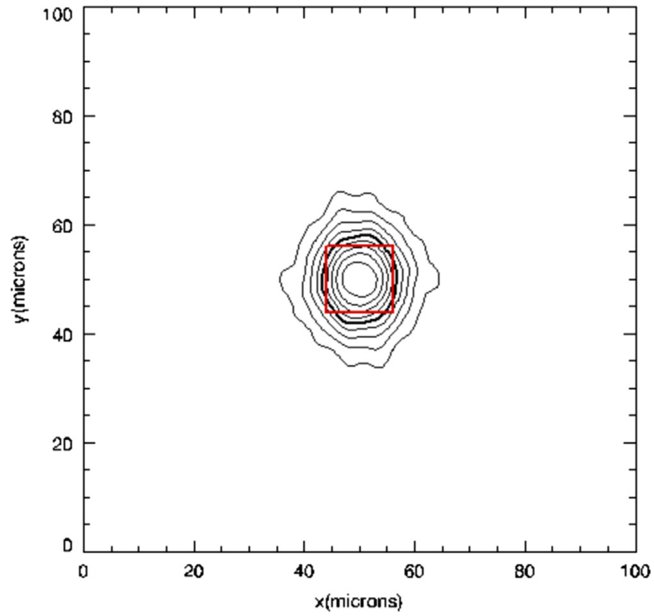

Fig. 8. The average pixel response function corresponding to an area of 512 × 512 pixels. The levels values go from 0 (the most outer) to 0.9. The “0.5-contour” (the FWHM) is plotted in bold.

Inside the pixel physical size, the average pixel response is almost circular. Outside the pixel, the response is asymmetric and dominated by the charges diffusion and the cross-talk between neighbouring pixels. This preliminary result also shows that the FWHM of the PRF is the same order of the pixel size.

5. Perspectives

The developments ongoing at the CEA target the development of a unique test bench for the IPSV characterizations of different detectors operating in VIS, NIR or LWIR ranges, by just changing the source and the CSIG. This test bench will permit to measure the intrapixel response of each individual pixel of a detector and then one can deduce the variation in intrapixel response at the scale of the detector.

To fulfill this requirement, a new characterization procedure will be implemented and it consists to scan, in front of the detector under test, the CSIG in *x*- and *y*-directions at an amplitude equal the period of the grating at step of pix/10. By this way, each individual pixel covered by the field of the CSIG would see one of its period and then the PRF of each pixel could be reconstructed. This approach has been validated by simulations considering a small area of 33 × 33 pixel and a CSIG amplitude displacement reduced to 12 μm with 1 μm step [11].

The first detector we plan to characterize is the visible detector (CCDs) for Euclid VIS Instrument. Euclid is a mission which targets to measure precisely the shapes of the galaxies [12] and then it can be interesting to evaluate sub-pixel responses of the flight version CCD. We plan also to characterize the NIR and LWIR detectors developed by the CEA-LETI.

To operate in the large spectrum domain (VIS to LWIR), the optical system of the final test bench would be constituted by achromatic mirrors all built in the same material to achieve the maximum mechanical stability. The coatings and the state of surfaces of elements will be specified carefully to minimize potential instrumental biases during the measurement. The baffling budget should also be considered with great attention to avoid spurious light typically during the characterizations in LWIR domain.

The cryostat could be a DN630 in Inox 304 with a Sumitomo type cryogenerator constituted by 2 stages delivering 5.4 W and 30 W, respectively, at 10 and 45 K.

We have received the funding from the DIM-ACAV and the LabEx P2IO, for the development of the test bench. This test bench will be available around the end-2015.

6. Conclusion

We have presented an original technique for the characterization of the intrapixel response of astronomical detectors. The technique consists in the projection of a highly spatially resolved pattern on the detector without optics but using the self-imaging property (Talbot effect) of a continuously self imaging grating (CSIG) illuminated by a plane wave. The technique has been evaluated on our preliminary test bench with the characterization of the e2v CCD-204. To know the spatial response of the detector with a precision of pix/10, we have designed a CSIG of 48 orders, to excite 1153 discrete spatial frequencies with a cutoff frequency value equal to 511 mm^{-1}. We have shown our aptitude to measure the modulation transfer function and also compute the average pixel response associated to 512×512 pixels considering zone. The average pixel response presents an asymmetry (elongation in one direction), which can be due to the presence of channel stops for the charge transfer in the CCD.

Acknowledgements

Following this study, the direct next steps will consist to evaluate the performance of the CCD-273 using the preliminary test bench. The detector is currently integrated in our cryostat and the electro-optics verifications are ongoing. The authors thank the European Spatial Agency for the loan of the CCD detectors (e2v 204 and 273).

This work has been partially supported by the LabEx FOCUS ANR-11-LABX-0013. The development of the final test bench is supported by the DIM-ACAV and the LabEx P2IO.

References

[1] J.G. Ingalls, J.E. Krick, S.J. Carey, S. Laine, J.A. Surace, W.J. Glaccum, C.C. Grillmair, P.J. Lowrance, Intra-pixel Gain Variations and High-precision Photmetry with the Infrared Array Camera (IRAC), SPIE (2012) 1.
[2] T.R. Lauer, Publications of the Astronomical Society of the Pacific 111 (765) (1999) 1434.
[3] D. Kavaldjiev, Z. Ninkov, Optical Engineering 37 (3) (1998) 948.
[4] A. Piterman, Z. Ninkov, Optical Engineering 41 (6) (2002) 1192.
[5] H. Toyozumi, M.C. Ashley, The Astronomical Society of Australia 22 (2005) 257.
[6] N. Barron, M. Borysow, K. Beyerlein, M. Brown, C. Weaverdyck, W. Lorenzon, M. Schubnell, G. Tarlé, A. Tomasch, Publications of the Astronomical Society of the Pacific (PASP) 119 (2007) 466.
[7] T.P.T.G. Biesiadzinski, M.J.S.M. Howe, W. Lorenzon, C. Weaverdyck, J. Larson, Proceedings of SPIE 7742 (77421M) (2010) 1.
[8] N. Guérineau, S. Rommeluère, E. di Mambro, I. Ribet, J. Primot, Comptes Rendus Physique 4 (2003) 1175.
[9] N. Guérineau, B. Harchaoui, J. Primot, K. Heggarty, Optics Letters 26 (7) (2001) 411.
[10] N. Guérineau, J. Primot, Journal of the Optical Society of America A: Optics, Image Science, and Vision 16 (2) (1999) 293.
[11] C. Ketchazo, T. Viale, O. Boulade, G. Druart, V. Moreau, L. Mugnier, D. Dubreuil, S. Derelle, S. Ronayette, N. Guérineau, M. Berthé, Proceedings of SPIE 9154 (91541Y) (2014).
[12] R. Laureijs, Euclid definition study report (2011).